Coherent stabilization of zero-electron-kinetic-energy states

Paolo Bellomo and C. R. Stroud, Jr.
Rochester Theory Center for Optical Science and Engineering and The Institute of Optics, University of Rochester, Rochester, New York 14627-0186

(Received 8 December 1998; accepted 20 January 1999)

The accuracy of zero-electron-kinetic-energy (ZEKE) photoelectron spectroscopy rests on the ultralong lifetimes of the high-n, high-l Rydberg states that are responsible for the ZEKE signal. However, a few-photon process cannot excite electrons directly from the low-l ground state to the high-l ZEKE manifold. In this paper we show that using the dynamics of Rydberg Stark states in slowly time dependent external fields it is possible to control coherently the angular momentum of Rydberg electrons, and therefore also their lifetime. We derive explicitly two different schemes based on simple, short electric dc pulses, which populate precisely those high-l, long-lived Rydberg states that are necessary for accurate ZEKE experiments. The high-l states that we construct are also Stark eigenstates, therefore a moderate dc external field can eventually enforce cylindrical symmetry and lock the ZEKE electrons in the stable, long-lived high-l manifold. © *1999 American Institute of Physics.* [S0021-9606(99)01515-9]

I. INTRODUCTION

In the past decade zero-electron-kinetic-energy photoelectron spectroscopy (ZEKE-PES or just ZEKE) has become the technique of choice for studying the spectra of molecular and cluster ions.[1–3] In ZEKE a laser pulse excites a core electron to some ultrahigh-n ($n \gtrsim 200$) Rydberg state just below the ionization threshold, or to a superposition of such states. Then follows a delay (typically μs), during which hot, non-ZEKE electrons leave the interaction region, and finally a dc electric pulse extracts the genuine ZEKE electrons from the molecule by field ionization. The same pulse also collects the ZEKE electrons, and their energy can be measured by time-of-flight methods. Note that the delay between the excitation of the high-n states, and the extraction of the ZEKE electrons is crucial to the accuracy of the experiment. It is during such delay that spurious, high energy electrons drift away from the interaction region, although Villeneuve *et al.*[4] have recently argued that some of them may remain trapped because of plasma effects.

The long-lived Rydberg states that are responsible for the ZEKE signal are known as ''ZEKE states,'' and the remarkable resolution of ZEKE stems directly from their existence and ultralong lifetimes. These states live considerably longer than expected based on a simple extrapolation from the computed lifetimes of low-n, low-l states. In any Rydberg manifold, it is only the low-l states that can be populated directly from the ground state by a few-photon process, whereas it is the high-l states that are the longest-living. Molecular Rydberg states typically decay by autoionization or by molecular dissociation. Both channels require some coupling of the Rydberg electron with the electronic states that are confined near to the molecular core, and such coupling becomes vanishingly small for high-l Rydberg states. When a Rydberg electron is placed in a high angular momentum state it experiences a centrifugal barrier, and the region in the proximity of the molecular core becomes classically forbidden. There, the wave function of the Rydberg electron decays exponentially, and so the coupling with the core electronic states (measured by the overlap with their wave function, which is sharply localized at the core) is vanishingly small, and that is why high-l Rydberg states are stable.

The early expectation that Rydberg lifetimes scale as $\sim n^3$ is in agreement with the classical picture, in which energy exchanges between the core and the electron take place only when the electron is at the perihelion, i.e., once per Kepler orbit (the classical Kepler period is $T_K = 2\pi n^3$). Simple quantum estimates, which are based on the magnitude of a low-l Rydberg wave function in the proximity of the core, yield the same scaling.[5,6] The arguments must be reassessed, however, in the light of experimental evidence that the lifetimes of ZEKE states are much longer, and may scale as the fifth power of n.[7–10] Clearly, high-l states are somehow accessed during the experiment, and this fortuitous circumstance is the practical reason why ZEKE is such a robust and widely used technique. The accidental stabilization of ZEKE states is probably due to a variety of factors, like stray dc fields[9,11–13] or the fields of neighboring ions,[10,13–20] which are always present in the molecular beam; intramolecular effects may also play a role.[21] Indeed, experimental evidence, and also theoretical arguments strongly suggest that collisions with ions are probably the most efficient vehicle for the population of large angular momentum states.

It is clear that the intramanifold dynamics of Rydberg electrons can be strongly influenced even by surprisingly weak fields. Mühlpfordt *et al.*[22] measured a moderate (up to a few μs) enhancement of the lifetime of DABCO in crossed electric and magnetic fields, which they interpreted theoretically by extensive classical trajectory Monte Carlo simulations. Ivanov and Stolow[23] have recently proposed a coherent control scheme, in which a Stark wave packet first evolves in a dc electric field. Next, when the expectation value of the angular momentum has become sufficiently

large, a crossed pulsed magnetic field is applied in order to lock the electron in the high-l manifold by changing the average magnetic quantum number of the state. However, their analysis is based on the dynamics of the expectation value of the angular momentum, and it does not yield an accurate estimate of how many ZEKE electrons remain trapped in the low-l, short-lived states. Jones *et al.*[24] studied the lifetimes of autoionizing Rydberg states of Ba in a circularly polarized microwave field. They observed lifetimes that were much longer than those measured in the presence of a linearly polarized microwave field. They also observed that these lifetimes approached a constant value near 70 ps for $n>18$. Bellomo *et al.*[25] used perturbative classical calculations to explain the findings of Ref. 24; they showed that for the values of the field parameters used in the experiment (i.e., field strength and rotation frequency) the Rydberg electron explores only a limited portion of the available classical phase space. More recently, Bellomo and Stroud[26] have corroborated that classical analysis by showing that a perturbative, classical trajectory Monte Carlo calculation is essentially equivalent to a full quantum treatment, in which the wave function is expanded over the basis of the coherent states of SO(4). Therefore, in principle circularly polarized microwave fields can be used for the enhancement of the lifetimes of Rydberg states, as long as the parameters of the field are chosen more judiciously, as Bellomo *et al.*[11] have already pointed out by classical arguments.

In this paper we use precisely the intramanifold dynamics of high-n Rydberg states in either a rotating electric field or an orthogonal dc pulse, to control coherently the state of the electron, and to populate the long-lived high-l states that are essential to ZEKE. That is, we propose two different explicit configurations of external fields, both of which will lock the ZEKE electron in the high angular momentum manifold (i.e., $l>4$). The dynamics takes place on a scale of a few nanoseconds, during which the decay due to the coupling with the core is not important. Once the electron is locked in a high-l state, it remains there almost indefinitely. More precisely, at the end of the time evolution the electron is in a superposition of high-l Stark eigenstates, and therefore an additional dc field can be quickly turned on to enforce cylindrical symmetry (as long as the applied field is much stronger than stray fields and the fields due to neighboring ions), and to lock the electron in the stable high-l manifold.

Our analysis is based on a simplified but representative hydrogenic model, which is very accurate for high-l states. We assume (see below) that the electron is initially excited to a Stark eigenmanifold, and that the external field is strong enough to effectively couple the low-l doorway state to the quasihydrogenic high-l manifold.

This paper is organized as follows: in Sec. II we briefly review the dynamics of Rydberg electrons in weak fields, and in Sec. III we derive explicitly two schemes for the stabilization of ZEKE states by slowly time dependent, weak electric fields. Finally, in Sec. IV we draw some general conclusions.

II. INTRAMANIFOLD DYNAMICS IN WEAK FIELDS

In this section we review the dynamics of Rydberg electrons in weak external fields. In atomic units, which we use throughout this paper, the Hamiltonian for a hydrogen atom in crossed electric and magnetic field reads

$$H=\frac{p^2}{2}-\frac{1}{r}+\frac{B}{2}L_y+Fz+\frac{B^2}{8}(x^2+z^2), \tag{1}$$

where the electric field is parallel to the z axis and its strength is F, whereas the magnetic field is parallel to the y axis, and its strength is B.

We consider the limit of weak fields, i.e., fields which do not mix adjacent Rydberg manifolds very much. Such limit holds when[5,6]

$$F<\frac{1}{3n^5} \quad \text{and} \quad B<\frac{1}{n^4}, \tag{2}$$

where n is the principal quantum number of the electron. That is, in this paper we assume that the external fields satisfy Eqs. (2), so that the dynamics is confined within a hydrogenic manifold to a reasonable approximation. Because the external fields are weak the diamagnetic term of the Hamiltonian, which is proportional to the square of the magnetic field, can be neglected. The simplified problem has been first solved quantum mechanically by Demkov *et al.*[27,28] However, their formal solution does not provide physical insight in the dynamics, and it makes it difficult to guess a field which will significantly enhance the angular momentum of a state. It also becomes computationally intractable in the limit of large n's.

The analysis of the intramanifold dynamics in the hydrogen atom is based on Pauli's replacement, which is an operator identity between the position operator $\hat{\mathbf{r}}$ and the scaled Runge-Lenz vector operator $\hat{\mathbf{a}}$ (throughout this paper we use boldface letters for vectors, and we indicate a quantum operator with a caret),[29,30]

$$\hat{\mathbf{r}}=-\tfrac{3}{2}n\hat{\mathbf{a}}, \tag{3}$$

where $\hat{\mathbf{a}}$ is a Hermitian operator, and for a bound state it is defined as

$$\hat{\mathbf{a}}=n\left\{\frac{1}{2}(\hat{\mathbf{p}}\times\hat{\mathbf{L}}-\hat{\mathbf{L}}\times\hat{\mathbf{p}})-\frac{\hat{\mathbf{r}}}{r}\right\}. \tag{4}$$

Pauli's replacement holds only within a hydrogenic n-manifold.

In the interaction representation and for fields of arbitrary orientation the Hamiltonian is

$$\hat{H}=-\boldsymbol{\omega}_S\cdot\hat{\mathbf{a}}-\boldsymbol{\omega}_L\cdot\hat{\mathbf{L}}, \tag{5}$$

where $\boldsymbol{\omega}_S=3n\mathbf{F}/2$ is the Stark frequency vector of the electric field, and $\boldsymbol{\omega}_L=-\mathbf{B}/2$ is the Larmor frequency vector of the magnetic field, and where we used Pauli's replacement and neglected the diamagnetic term. We define the Larmor frequency with a minus sign, so that the dynamics is formally identical to that of a negative charge in a noninertial frame, rotating with frequency $\boldsymbol{\omega}_L$. The simplified Hamil-

tonian of Eq. (5) has proven to be surprisingly accurate, and it accounts for several experimental results.[11,17,18,25,31]

It is customary to introduce the following operators:

$$\hat{\mathbf{J}}_1=\tfrac{1}{2}(\hat{\mathbf{L}}+\hat{\mathbf{a}}), \quad \hat{\mathbf{J}}_2=\tfrac{1}{2}(\hat{\mathbf{L}}-\hat{\mathbf{a}}). \tag{6}$$

It is well known that $\hat{\mathbf{J}}_1$ and $\hat{\mathbf{J}}_2$ commute with each other and that their components constitute a realization of the angular momentum algebra.[30] Furthermore, the Hamiltonian can be rewritten in terms of $\hat{\mathbf{J}}_1$ and $\hat{\mathbf{J}}_2$,

$$\hat{H}=-\boldsymbol{\omega}_1\cdot\hat{\mathbf{J}}_1-\boldsymbol{\omega}_2\cdot\hat{\mathbf{J}}_2, \tag{7}$$

where

$$\boldsymbol{\omega}_1=\boldsymbol{\omega}_L+\boldsymbol{\omega}_S, \quad \boldsymbol{\omega}_2=\boldsymbol{\omega}_L-\boldsymbol{\omega}_S. \tag{8}$$

Equation (7) reduces the problem to the dynamics of two uncoupled spins in the external ''magnetic fields'' $\boldsymbol{\omega}_1$ and $\boldsymbol{\omega}_2$. Finally, $\hat{\mathbf{L}}$ and $\hat{\mathbf{a}}$ obey two constraints,

$$\hat{\mathbf{L}}\cdot\hat{\mathbf{a}}=0, \quad \hat{\mathbf{L}}^2+\hat{\mathbf{a}}^2=n^2-1, \tag{9}$$

and one has

$$\hat{\mathbf{J}}_1^2=\hat{\mathbf{J}}_2^2=j(j+1), \quad 2j+1=n. \tag{10}$$

Using the operators $\hat{\mathbf{J}}_1$ and $\hat{\mathbf{J}}_2$ is equivalent to solving the Kepler problem in parabolic coordinates. That is, the eigenstates of the hydrogenic Hamiltonian in parabolic coordinates are also the eigenstates of the two angular momentum operators $\hat{\mathbf{J}}_1^2$ and $\hat{\mathbf{J}}_2^2$, which are really one and the same operator [see Eqs. (10)], and of their projections along the z axis, $\hat{J}_{1,z}$ and $\hat{J}_{2,z}$. Those very same states are also the familiar $|nkm\rangle$ Stark eigenstates of the hydrogen atom in a weak electric field. Formally,

$$|nkm\rangle=|j_1m_1\rangle\otimes|j_2m_2\rangle=|j_1j_2;\ m_1m_2\rangle, \tag{11}$$

where $j_1=j_2=j$, and k and m are, respectively, the electric and magnetic quantum number, and they are, respectively, the eigenvalues of $\hat{a}_z$ and $\hat{L}_z$. The relationship of k and m with the quantum numbers of $\hat{J}_{1,z}$ and $\hat{J}_{2,z}$, i.e., m_1 and m_2 is

$$k=m_1-m_2, \quad m=m_1+m_2. \tag{12}$$

Finally, the relationship between n and j is given in the second of Eqs. (10).

In Fig. 1 we show a *schematic* representation on the unit sphere of a Stark state with $m=0$. The state corresponds to two ensembles of classical vectors $\mathbf{J}_1$ and $\mathbf{J}_2$, with a sharply defined projection along the z axis. These classical vectors have projections on the xy plane that point in all possible directions, which reflects the quantum uncertainty on the x and y components of the angular momentum when the state is quantized along the z axis. Therefore the classical vectors of the ensembles, which represent an $m=0$ Stark state, describe a pair of cones that share their symmetry axis but point in opposite directions. Angular momentum eigenstates $|jm\rangle$ are often represented on the unit sphere by spherical harmonics, however this is possible only for *integer* j and m,[32] whereas in the parabolic eigenstates of hydrogen one may also have *half-integer* quantum numbers, as one can see from the second of Eqs. (10), and that is why a semiclassical representation is necessary.

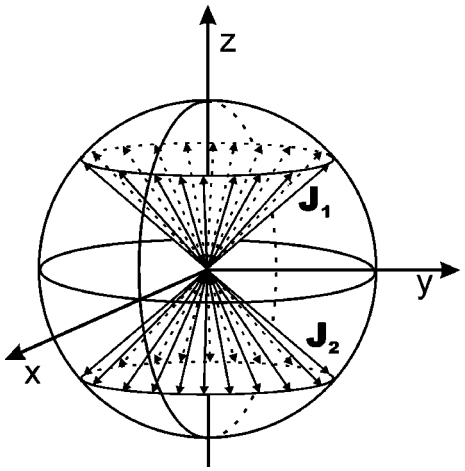

FIG. 1. Schematic representation of a Stark state with $m=0$. This state is the direct product of two eigenstates respectively of $\hat{\mathbf{J}}_1^2,\hat{J}_{1,z}$ and $\hat{\mathbf{J}}_2^2,\hat{J}_{2,z}$. These two eigenstates have opposite projections along the z axis. Angular momentum states can be represented semiclassically on the unit sphere by an ensemble of classical vectors, the projections of which along the z axis are sharply defined, whereas their projections on the xy plane are distributed uniformly in all directions. Therefore, a $m=0$ Stark eigenstate is represented by a pair of cones, which have the same axis of symmetry, but point respectively along the positive and negative z axis. In the actual classical distribution there is still some fuzziness on the z axis (which we do not show explicitly for the sake of a less crowded figure), because in a semiclassical representation an integer quantum number corresponds to a finite window of classical values.

We conclude this section establishing the connection between the Stark states and the more familiar $|nlm\rangle$ eigenstates of the hydrogen atom in polar coordinates.

By summing two angular momentum operators one obtains an alternative complete set of commuting observables,

$$\begin{aligned}&\hat{\mathbf{J}}^2=(\hat{\mathbf{J}}_1+\hat{\mathbf{J}}_2)^2,\\ &\hat{\mathbf{J}}_z=\hat{\mathbf{J}}_{1,z}+\hat{\mathbf{J}}_{2,z},\\ &\hat{\mathbf{J}}_1^2, \quad \hat{\mathbf{J}}_2^2.\end{aligned} \tag{13}$$

The eigenstates of the new set of observables are connected to the old ones by Clebesch–Gordan coefficients[33]

$$|j_1j_2;\ jm\rangle = \sum_{m_1}\sum_{m_2}\langle j_1j_2;\ m_1m_2|j_1j_2;\ jm\rangle|j_1j_2;\ m_1m_2\rangle, \tag{14}$$

where again $j_1=j_2=j$. The states $|j_1j_2;\ jm\rangle$ are precisely the familiar $|nlm\rangle$ eigenstates of the hydrogen atom in polar coordinates, and therefore Eq. (14) expresses the connection between the spherical and the parabolic (i.e., Stark) eigenbases.[30,34]

III. STABILIZATION OF ZEKE STATES

Our methods of locking a Rydberg electron in the stable high-l manifold are based on the dynamics of hydrogenic Stark eigenstates in time dependent external fields. That is,

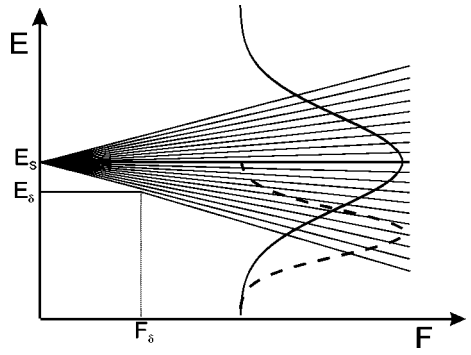

FIG. 2. Schematic representation of the Stark manifold and of the width of the laser pulse (continuous line). We assume that the applied Stark field is greater than F_δ, i.e., the field necessary to mix the low-l doorway state with the hydrogenic Stark manifold, and that the width of the pulse is large enough to excite several states in the manifold. This means that the excitation pulse must be much shorter than the Stark period of the applied dc field. In the figure we also show an ''ideal'' pulse, which excites preferentially the red Stark states (dashed line). As we explain in the main text, the stabilization method based on a rotating electric field is more effective when the excitation process does not populate the low-k Stark states at the center of the Stark manifold.

we assume that when the initial few-photon process excites the electron to the desired Rydberg level a dc electric field $\mathbf{F_0}$ is also applied, therefore we assume that the electron is really excited to a superposition of Stark eigenstates. We consider the case of Stark states with $m=0$, however, it is easy to see that our analysis can be extended to the case of nonzero, small m's. Clearly, we must require that the applied dc field is strong enough to mix the low-l doorway state with the quasi degenerate high-l Stark manifold, that is,[6]

$$F_0 \geqslant F_\delta = \frac{2}{3}\frac{\delta_l}{n^5}, \tag{15}$$

where δ_l is the quantum defect of the doorway state, and $|\delta_l| \leqslant 0.5$.

Furthermore, we assume that the width of the laser pulse is large enough to excite a significant fraction of the Stark manifold, and not just a single Stark state, as we show schematically in Fig. 2. Indeed, this assumption is not strictly necessary, especially for the method based on a slowly rotating field (see below), however, it is very realistic, because for very large principal quantum numbers the width of a typical laser pulse does not resolve the individual Stark levels. In short, we assume that when the laser pulse vanishes (at time $t=0$), several $m=0$ Stark states are populated, and also that the Stark dc field is still applied.

Because the goal is the enhancement of the angular momentum of the state, it might seem more appropriate to describe the dynamics in the basis of the eigenstates of $\hat{\mathbf{L}}^2$, i.e., the spherical eigenstates $|nlm\rangle$. However, that is not the case, because the time evolution is much simpler when it is expressed in terms of the Stark eigenstates, as we show more in detail below. Furthermore, the Stark eigenstates are also eigenstates of $\hat{L}_z$, and an increase in m is enough to impose a lower bound on the total angular momentum, because $l \geqslant m$. The accuracy of ZEKE does not depend on the specific value of the angular momentum, but rather on the existence of a lower bound on it (typically $l>4$), so that the Rydberg state has vanishing overlap with the short lived, low-l states. Such lower bound can be obtained as well by enhancing m rather than l, and that is why it is convenient to work in the Stark eigenbasis.

A glance at Fig. 1 reveals immediately what must be done to enhance the projection of the angular momentum along some spatial direction. That is, one must construct a field in which the cones of Fig. 1, which represent schematically a Stark state, evolve in time so that their symmetry axes eventually overlap one another. Moreover, and unlike in Fig. 1, at the final time the two cones must also *point in the same direction* so to maximize the sum of the projections of the effective angular momenta $\mathbf{J}_1$ and $\mathbf{J}_2$ along the axis of the cones. Clearly, the two ensembles of classical vectors evolve in time only if one varies the orientation of the Stark field, and not only its magnitude, because in a field with constant orientation a Stark state remains an eigenstate of the system, and the field changes only the phase of the state. Indeed, the vectors of the classical ensembles precess, respectively, around $\boldsymbol{\omega}_1$ and $\boldsymbol{\omega}_2$, i.e., the effective ''magnetic fields'' of the Hamiltonian of Eq. (7).[11,35] If the orientation of $\boldsymbol{\omega}_1$ and $\boldsymbol{\omega}_2$ is constant, then the tips of the classical vectors $\mathbf{J}_1$ and $\mathbf{J}_2$ simply move along the rims of two cones of Fig. 1, and therefore the ensembles themselves are invariant. However, if the orientation of the Stark field varies then the axes of precession are time dependent, and the two cones evolve in time.

Although the distributions of the classical vectors $\mathbf{J}_1$ and $\mathbf{J}_2$ represent a Stark state only schematically, the intuitive picture of the dynamics, which we have outlined above, holds also at a more formal level. The Hamiltonian of Eq. (7) is a linear combination of effective angular momentum operators, i.e., the generators of the rotation group, therefore the time evolution of the states $|j_1 m_1\rangle \otimes |j_2 m_2\rangle$ is given by two independent rotations, which operate respectively on $|j_1 m_1\rangle$ and $|j_2 m_2\rangle$. The magnitude of the projection of $\hat{\mathbf{L}}$ on a given axis is much larger when $|j_1 m_1\rangle$ and $|j_2 m_2\rangle$ are quantized along that axis and also ''point in the same direction,'' i.e., m_1 and m_2 have the same sign [see Eqs. (12)]. When the axes of the two cones of classical vectors are aligned, it means precisely that the eigenstates of the two angular momenta are quantized along the same axis, and when the two cones point in the same direction it means that every Stark state with $m=0$ has evolved in time as follows:

$$|j_1 j_2;\ m_1 m_2 = -m_1\rangle \Rightarrow |j_1 j_2;\ m_1' m_2' = +m_1'\rangle, \tag{16}$$

where $j_1 = j_2 = j$, and where

$$|m_1'| = |m_1| \quad \text{and} |m_2'| = |m_2|. \tag{17}$$

Finally, the prime indicates that the axis of quantization has changed.

According to Eqs. (12) and Eq. (16) the magnitudes of the projection on the new axis, respectively, of the Runge–Lenz vector and of the angular momentum are

$$\begin{aligned} |k'| &= |m_1' - m_2'| = 0, \\ |m'| &= |m_1' + m_2'| = 2|m_1|. \end{aligned} \tag{18}$$

The $m=0$ Stark manifold contains $2j+1=n$ states [see Eqs. 10], with $-j\leqslant m_1\leqslant j$, and with $m_2=-m_1$. After the time evolution, the lower bound $l>4$ is broken only by those Stark states that finally have $m_1'=0,\pm 1,\pm 2$, for integer j. Assuming as a first approximation that the Stark states are populated uniformly, the probability to find the Rydberg electron in a low-m' Stark state, which may have nonvanishing overlap with the short lived low-l states, is

$$P(|m'|\leqslant 2)=\frac{5}{n}, \tag{19}$$

which becomes rapidly negligible for increasing n. Furthermore, the final states are again Stark states, and a small magnetic quantum number m' does not necessarily imply that the state has a low-l character. That is, these low-m' Stark states are still superpositions of *all* the $|nlm\rangle$ states [see Eq. (14)], and therefore the probability that the electron is in a short lived, low-l state is diluted by yet another factor $\sim 1/n$.

It is easy to see from Eq. (16) that it is the low-k initial Stark states that evolve into the final low-m' states. Therefore, an ''ideal'' laser pulse should excite preferentially the red (or blue) Stark states, and it should not populate significantly the low-k states at the center of the Stark manifold (see Fig. 2). When that happens, at the end of the time evolution the Rydberg electron is almost perfectly locked in the high-m' manifold, and therefore it is almost perfectly stable.

A. Stabilization by a rotating field

Our first prescription for a slowly time dependent field, in which the cones of Fig. 1 eventually align their axes pointing in the same direction, is nothing other than a prescription for turning off the initial Stark field judiciously. That is, as we turn off the field we also let it *rotate* around the y axis. This is equivalent to turning off the field along the z axis while applying a suitable dc pulse along the x axis. Therefore, our prescription is

$$\mathbf{F}(t)=F(t)\left[\cos\left(\int_0^t \omega_R(t')dt'\right)\mathbf{n}_z + \sin\left(\int_0^t \omega_R(t')dt'\right)\mathbf{n}_x\right], \tag{20}$$

where $\mathbf{n}_z$ and $\mathbf{n}_x$ are, respectively, unit vectors along the z and x axis, and $\omega_R(t)$ is the time dependent rotation frequency. At the initial time $t=0$ our field is the same as the initial Stark field, i.e.,

$$\mathbf{F}(0)=\mathbf{F}_0. \tag{21}$$

We also set a final time τ, which must be long compared to the Kepler period to insure that the motion is confined within an n-manifold. We require that at such time τ the field vanishes, so that the evolution of the electronic state halts

$$F(\tau)=0. \tag{22}$$

The dynamics of a Stark state in the field of Eq. (20) is best analyzed in a frame rotating with the field. A rotating frame is not a Galilean frame, and the inertial effects of the Coriolis forces can be described exactly by introducing an effective Larmor frequency equal to the rotation frequency $\boldsymbol{\omega}_R$ of the frame of reference.[17,28,36] The analysis of the preceding section applies exactly, with the following substitution:

$$\boldsymbol{\omega}_L \Rightarrow \boldsymbol{\omega}_R, \tag{23}$$

and for the field of Eq. (20) $\boldsymbol{\omega}_R$ points along the positive y axis. We also require that at all times

$$\omega_R(t)=\omega_S(t). \tag{24}$$

The condition of Eq. (24) favors the desired large variations of the angular momentum of the state. It has been shown in Refs. 11,17 that crossed electric and magnetic fields (or a rotating electric field) change the angular momentum of a state most efficiently when the Stark and Larmor (or rotation) frequencies are of comparable magnitude. This observation has already been demonstrated, although indirectly, by the experimental results of Jones *et al.*,[24] and also by the theoretical interpretation of those results by Bellomo *et al.*,[25] which show that the lifetimes of Rydberg states in circularly polarized microwave fields remain constant, with increasing principal quantum number, when the rotation frequency of the field becomes much larger than the Stark frequency.

Equation (24) means that the ''magnetic fields'' $\boldsymbol{\omega}_1$ and $\boldsymbol{\omega}_2$ of the Hamiltonian of Eq. (7) have constant orientation in space, and that only their magnitude changes in time. That is,

$$\boldsymbol{\omega}_i=\omega_i(t)\mathbf{n}_{\omega_i}, \quad \mathbf{n}_{\omega_i}=(\tilde{\omega}_{ix},\tilde{\omega}_{iy},\tilde{\omega}_{iz}) \quad i=1,2, \tag{25}$$

where $\tilde{\omega}_{ix}$, $\tilde{\omega}_{iy}$, and $\tilde{\omega}_{iz}$ are the components of the unit vector $\boldsymbol{n}_{\omega_i}$ that points along $\boldsymbol{\omega}_i$. In that case, the Hamiltonian at a time t commutes with itself at a different time, that is,

$$[H(t),H(t')]=0, \tag{26}$$

and the propagator is simply

$$\hat{U}(t,0)=e^{i\mathbf{n}_{\omega_1}\cdot\hat{\mathbf{J}}_1\int_0^t\omega_1(t')dt'}e^{i\mathbf{n}_{\omega_2}\cdot\hat{\mathbf{J}}_2\int_0^t\omega_2(t')dt'}. \tag{27}$$

The propagator of Eq. (27) is the product of two rotations, which operate, respectively, on the two subspaces spanned by the eigenvectors of $\hat{\mathbf{J}}_1^2,\hat{J}_{1,z}$ and $\hat{\mathbf{J}}_2^2,\hat{J}_{2,z}$. Therefore, the states $|j_1m_1\rangle$ and $|j_2m_2\rangle$, respectively, *precess* clockwise around the ''magnetic fields'' $\boldsymbol{\omega}_1$ and $\boldsymbol{\omega}_2$. For the field of Eq. (20) both ''magnetic fields'' lie in the yz plane; $\boldsymbol{\omega}_1$ bisects the angle between the $+y$ and $+z$ axes, whereas $\boldsymbol{\omega}_2$ bisects the angle between the $+y$ and $-z$ axes. The angle of precession depends on the magnitude of the ''magnetic fields,'' which is one and the same, and we require that at final time τ the angle of precession is equal to an odd integer multiple of π, that is,

$$\int_0^\tau\sqrt{\omega_S^2(t)+\omega_R^2(t)}dt=\sqrt{2}\int_0^\tau\omega_R(t)dt=(2p+1)\pi, \tag{28}$$

where p is some integer. Equation (28) fixes the total angle of precession of the states and also the total angle of rotation of the field.

The action of the propagator on the Stark states can be expressed in terms of Wigner rotation matrices,[33] but a geometric interpretation is also possible and more desirable. It is easy to see from Fig. 3 that a vector oriented along the $+z$

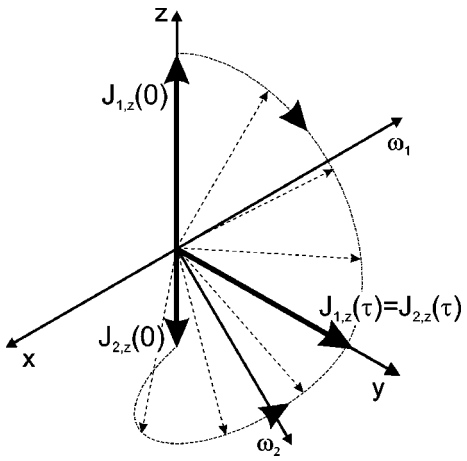

FIG. 3. Dynamics in the rotating frame of the axis of the cones which represent a Stark state. The axes of the cones correspond to the z projection of the angular momenta $\mathbf{J}_1$ and $\mathbf{J}_2$, and so we represent them as two vectors, $J_{1,z}$ and $J_{2,z}$. The external field satisfies the requirements described in the text, with $p=0$. At time $t=0$ the two vectors point respectively along the $+z$ and $-z$ axis. Next, they precess clockwise, respectively, around the two axes $\boldsymbol{\omega}_1$ and $\boldsymbol{\omega}_2$ (which lie in the yz plane), and at the final time τ both vectors are aligned along the y axis. The dashed curved lines show the trajectories described by the tips of $J_{1,z}$ and $J_{2,z}$, while the dashed arrows represent the same vectors at some intermediate times. From the point of view as shown in the figure, $J_{1,z}$ precess *behind* its axis of rotation $\boldsymbol{\omega}_1$, whereas $J_{2,z}$ passes *in front of* $\boldsymbol{\omega}_2$.

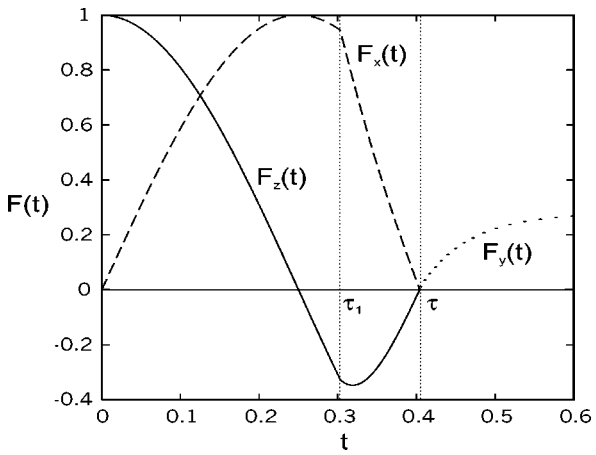

FIG. 4. Components of the time dependent field of Eq. (31) that enhances the angular momentum of the electron according to our first scheme. The units are arbitrary, and the maximum field strength and the associated Stark period are set equal to 1. The rotating field of Eq. (31) is equivalent to two crossed dc fields pointing, respectively, in the z (continuous line) and x (dashed line) directions, and we set $p=0$. The two vertical dotted lines marks the time $t=\tau_1$, when the magnitude of the field begins to decrease and the quadratic chirp is turned on, and the time $t=\tau$ when the field vanishes. In the figure we also show a final, weak dc field along the y axis (dotted line), which enforces cylindrical symmetry and locks the electron in the high-l manifold.

axis, and precessing clockwise around $\boldsymbol{\omega}_1$ by an angle π (or by an odd integer multiple of π) eventually overlaps with the y axis. The same holds for a vector pointing along the $-z$ axis and precessing around $\boldsymbol{\omega}_2$ by the same angle. Therefore, the quantum propagator acts on the $m=0$ Stark states as follows:

$$\hat{U}(\tau,0)|j_1 m_1\rangle\otimes|j_2 m_2=-m_1\rangle=|j_1 m_1'\rangle\otimes|j_2 m_2'=+m_1'\rangle, \tag{29}$$

where $j_1=j_2=j$, and the new axis of quantization is the y axis. Note that the y axis is the axis of rotation of the rotating frame, and so it coincides with the y axis of the inertial frame, i.e., the frame of the laboratory.

Eventually, the whole $m=0$ Stark manifold transforms as follows:

$$\{|nk0\rangle,-(n-1)\leqslant k\leqslant n-1\}$$
$$\Rightarrow\{|n0m'\rangle,-(n-1)\leqslant m'\leqslant n-1\}, \tag{30}$$

and the electron is in a superposition of high-m Stark eigenstates quantized along the y axis. Therefore, a Stark field can be quickly turned on along the y axis to enforce cylindrical symmetry, and to lock the electron in the desired long-lived high-l ZEKE states.

As an example we consider a specific functional form for the amplitude of the field, and also for the rotation frequency (see Fig. 4),

$$\boldsymbol{F}(t)=F_0\left[1-\frac{t-\tau_1}{\tau-\tau_1}\theta(t-\tau_1)\right]$$
$$\times[\cos\phi(t)\boldsymbol{n}_z+\sin\phi(t)\boldsymbol{n}_x], \tag{31}$$

where τ_1 is some intermediate time in the interval $[0,\tau]$, and θ is the step function. The angle $\phi(t)$ is

$$\phi(t)=\frac{3n}{2}F_0\left[t-\frac{(t-\tau_1)^2}{2(\tau-\tau_1)}\theta(t-\tau_1)\right], \tag{32}$$

that is, the field initially rotates with a linear phase, and a quadratic chirp is turned on at $t=\tau_1$. If we assume $\tau_1=3\tau/4$ then the condition of Eq. (28) becomes

$$\tau=(2p+1)\frac{2^{3/2}T_S(F_0)}{7}, \tag{33}$$

where $T_S(F_0)$ is the Stark period of F_0. For $n=100$, $p=0$, and F_0 equal to half the Inglis–Teller limit, i.e., $F_0=1/6n^5$ (that is, $F_0\approx 0.1$ V/cm), one has $\tau\approx 25$ ns. That is a time scale over which it begins to be difficult to obtain good control over the field. Clearly, the total time depends crucially on the strength of the initial field, and weaker fields correspond to longer times, over which the field can be controlled more accurately. However, one cannot weaken the external field arbitrarily, because the lower bound imposed by the quantum defect must always be considered. The time scale can be increased by using a different functional form for the field, or by selecting higher principal quantum numbers, or more simply by considering a larger half-integer number of Stark–Larmor oscillations, that is, a larger integer p.

B. Stabilization by an orthogonal pulse

As a second scheme, we discuss a method similar to the two-pulses schemes of Refs. 23, 37. This second scheme can also be interpreted in terms of the precession of the states $|j_1 m_1\rangle$ and $|j_2 m_2\rangle$. Indeed, it is easy to see that after the

original Stark field along the z axis has been switched off, a second pulse along the x axis may also align the two cones representing a Stark state on the y axis.

More precisely, we assume that the two fields do not overlap in time, that is, we turn on the field along the x axis only after switching off (almost) completely the original Stark field. The time evolution is dictated first by the original Stark field alone, and next the precession of the states is determined solely by the dc pulse along the x axis. While we turn off the original Stark field there is no precession, because the original Stark states are quantized exactly along the axis of the field. The actual precession of the states $|j_1 m_1\rangle$ and $|j_2 m_2\rangle$ takes place only later, when the orthogonal field is applied. There is no crossed Larmor frequency, and the axes of precession are determined only by the Stark frequency of the orthogonal pulse, therefore their spatial orientation is trivially constant. The quantum propagator is still given by the simple expression of Eq. (27), and it still consists of two rotation operators acting on two separate subspaces. In the ''magnetic fields'' of Eqs. (8) the Stark frequency appears with opposite signs, and so the states $|j_1 m_1\rangle$ and $|j_2 m_2\rangle$ precess in opposite directions. A *clockwise* rotation of $|j_1 m_1\rangle$ around the x axis is matched by a *counterclockwise* rotation of $|j_2 m_2\rangle$ around the same axis. If the total angle of precession is chosen exactly equal to $\pi/2$ (or to an odd integer multiple of $\pi/2$), both states eventually align along the y axis, with m_1' and m_2' having the same sign, as in Eq. (16).

In this second scheme we impose requirements on the area of the dc pulses. Let τ_1 be the intermediate time when the original Stark field vanishes, and the orthogonal pulse begins to rise; we require that

$$\int_0^{\tau_1} F_1(t)\,dt = (2p+1)\frac{\pi}{3n}, \qquad \int_{\tau_1}^{\tau} F_2(t)\,dt = (2q+1)\frac{\pi}{3n}, \tag{34}$$

where p and q are integers, and where $F_1(t)$ is the magnitude of the original Stark field, which we assume to be constant until $t=0$, and $F_2(t)$ is the magnitude of the dc pulse along the x axis. At the final time τ the second pulse also vanishes, and the evolution of the states halts.

The laser pulse which excites the Rydberg electron is much shorter than the Stark period, because we assume that its bandwidth is large enough to excite the whole manifold, or a significant fraction of it, and therefore the Stark evolution can be neglected while the laser pulse is applied. Right after the pulse, the electron is in a superposition of Stark states, i.e., a Stark wave packet, which is approximately equal to the low-l, spherical state that is coupled to the ground state by the optical field. The first constraint of Eqs. (34) means that at time $t=\tau_1$ the Stark wave packet has completed a half-integer number of Stark oscillations, and the electron has a large angular momentum. That is, the Stark field couples the low-l doorway state to the high-l manifold, and after a half-integer number of Stark oscillations the population of the high-l states is at a maximum.

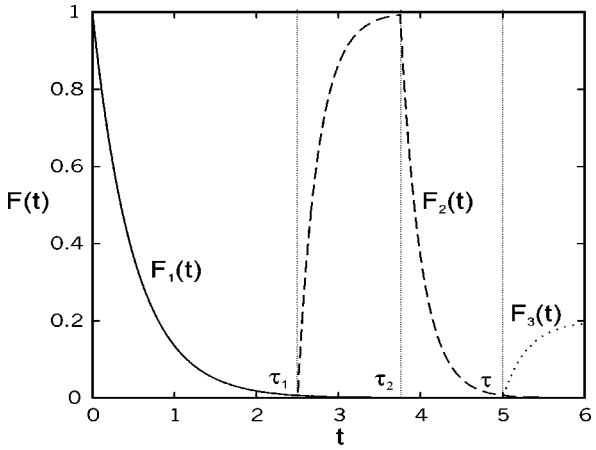

FIG. 5. Magnitude of the time dependent fields of Eqs. (35) and (38) for the second scheme based on an orthogonal pulse. The units are arbitrary, and the maximum field strengths and the associated Stark periods are set equal to 1. The parameters of the fields were set as is described in the main text, with $F_{0,1}=F_{0,2}=1$, and the integers p and q were, respectively, equal to 0 and 2. The original Stark field $F_1(t)$ (continuous line) points along the z axis, whereas the orthogonal dc pulse $F_2(t)$ (dashed line) points along the x axis. The vertical dotted lines mark the times τ_1, τ_2, and τ, which are defined in the main text. In the figure we also show a final, weak dc field $F_3(t)$ (dotted line) along the y axis, which enforces cylindrical symmetry and locks the electron in the high-l manifold.

As the first field vanishes, the second dc pulse kicks in, and the states $|j_1 m_1\rangle$ and $|j_2 m_2\rangle$ begin to precess. The second constraint of Eqs. (34) means that at the end of the precession both states are aligned along the y axis, with m_1' and m_2' having the same sign, and the electron is locked in the high-m manifold. Note that eventually the second field must be turned off to achieve maximum efficacy, so that the precession halts at the right time, and this is a fundamental difference with respect of the scheme proposed by Baranov *et al.*[37] Moreover, the constraints of Eqs. (34) also differentiate substantially our method from that proposal of Ref. 37, in which the authors suggest that the direction of the field should be changed as quickly as possible. In fact, in the accompanying experimental paper[38] Baranov *et al.* do turn off their second dc field, and the actual rise times and durations of their fields are such that the area under the pulses is of the same order of magnitude as the Stark periods, so that Eqs. (34) are approximately satisfied.

After the orthogonal pulse has vanished, the final states are high-m Stark states quantized along the y axis, and a final, weak dc field along the y axis can be used to enforce cylindrical symmetry, and to lock the electron in the high-l manifold.

As an example, and to obtain some quantitative estimates of the fields strengths and time scales involved, we assume that we turn off the original Stark field in the simplest way, i.e., by exponential decay (see Fig. 5),

$$F_1(t) = F_{0,1} e^{-t/\beta_1}, \tag{35}$$

where $F_{0,1}$ is the amplitude of the original Stark field, β_1 is a time constant, and $\beta_1 \lesssim \tau_1/5$ (recall that τ_1 is the intermediate time when the original Stark field vanishes, and the orthogonal dc field is turned on). The first constraint of Eqs. (34) yields

$$\beta_1 F_{0,1}[1-e^{\tau_1/\beta_1}] \approx \beta_1 F_{0,1} = (2p+1)\frac{\pi}{3n}, \tag{36}$$

from which it follows:

$$\beta_1 = (2p+1)\frac{\pi}{3nF_{0,1}} = (2p+1)\frac{T_S(F_{0,1})}{4}, \tag{37}$$

where $T_S(F_{0,1})$ is the Stark period of the original Stark field. Given the simplicity of the field, we may consider shorter times, that is, smaller principal quantum numbers. If we assume $n=50$, which is at the lower edge of Rydberg states that may be used in ZEKE, and for an initial Stark field at half the Inglis–Teller limit, i.e., $F_{0,1}=1/6n^5$ (that is, $F_{0,1}\approx 3$ V/cm), the Stark period is $T_S(F_{0,1})\approx 4$ ns. That is a time scale over which it is difficult to obtain good control over the field, although the functional form of Eq. (35) is particularly simple.

Next, we consider a dc pulse along the x axis of amplitude $F_{0,2}$, and again we assume exponential rise and decay with time constant β_2 (see Fig. 5),

$$F_2(t) = F_{0,2}\{[1-e^{-(t-\tau_1)/\beta_2}]\theta(\tau_2-t) + [1-e^{-(\tau_2-\tau_1)/\beta_2}]e^{-(t-\tau_2)/\beta_2}\theta(t-\tau_2)\}\theta(t-\tau_1), \tag{38}$$

where θ is the step function, and τ_2 is the midpoint of the time interval $[\tau_1,\tau]$. The field must vanish at $t=\tau$, and we so set $\beta_2 \lesssim (\tau-\tau_2)/5$. The second constraint of Eqs. (34) yields

$$F_{0,2}\{(\tau_2-\tau_1)-\beta_2 e^{-(\tau-\tau_2)/\beta_2}[1-e^{-(\tau_2-\tau_1)/\beta_2}]\} \approx F_{0,2}(\tau_2-\tau_1) = (2q+1)\frac{\pi}{3n}, \tag{39}$$

which means that

$$\beta_2 \lesssim (2q+1)\frac{T_S(F_{0,2})}{20}. \tag{40}$$

For $q=0$ and for a field equal to half the Inglis–Teller limit one has $\beta_2 \lesssim 0.2$ ns.

Again, the time scales can be increased to experimentally more convenient lengths by using weaker external fields. However, as we mentioned before, the lower bound imposed by the quantum defect must always be considered. Alternatively, the rise times and durations of the fields can be modified by selecting a different functional form for the fields, or a Rydberg manifold with larger principal quantum number. Finally, a larger value of the integers p and especially q will also make the precise control of the field parameters more feasible.

IV. CONCLUSIONS

In this paper we have presented two schemes for the enhancement of the angular momentum of Stark Rydberg states. Both methods are based on the intramanifold dynamics of high-n hydrogenic states in weak external fields, and the enhancement of the angular momentum takes place on a very short time scale, of the order of a few nanoseconds. ZEKE states are high-l Rydberg states, and therefore our schemes constitute two simple ways to populate precisely those Rydberg states that contribute most to the ZEKE signal. Similar fields configurations were also discussed in the context of the dynamics of the coherent states of SO(4).[26,39] In standard ZEKE experiments one populates several very high-n Rydberg manifolds, rather than just one manifold with a relatively low principal quantum number. Under present conditions using a low-n Rydberg manifold is not practical, because such low-n states do not live long enough under usual experimental techniques. However, the schemes which we have described would enhance precisely the lifetime of an individual low-n Rydberg state, and so one could possibly extend the application of some ''ZEKE-like'' methodology also to the region of lower n.[37,40]

The fields that we propose transform an $m=0$ Stark manifold into another Stark manifold, which is quantized along an orthogonal direction. The new Stark states also have well defined angular momentum along the new axis of quantization, and for most of these states the angular momentum is so large that it effectively quenches the coupling between the Rydberg electron and the core. In both schemes at some selected time the external fields must be turned off, so that the evolution of the states halts exactly when the electron is confined in the high-l manifold. Then, stray fields and the fields of neighboring ions could, in principle, scramble the angular momentum of the electron and transfer population back into the low-l states. However, that is not a problem. Stray and ionic fields are very weak and their Stark periods are very long, so that the scrambling of the angular quantum numbers takes place on a very long time scale. On the other hand, because in our schemes the final states are high-m Stark eigenstates, eventually one can turn on a final dc field with a very short rise time, and which points along the axis of quantization of the states. The applied dc field, which can easily be much stronger than the ultraweak stray and ionic fields, enforces cylindrical symmetry and so it locks the electron in the high-l manifold for good.

The first scheme makes use of a slowly rotating field, and it is based on the dynamics of the individual Stark states. Therefore, the details of the excitation of the Rydberg Stark manifold are irrelevant. The constraints on the field strength, and rotation frequency may be difficult to match for very short Stark periods with current technology, and the method is more easily feasible for larger principal quantum numbers. However, there is no need for a perfect match between field strength and rotation frequency, because in ZEKE one is not concerned with the population of some specific high-l state, but rather with the generic enhancement of the Rydberg lifetimes. The same consideration holds for the resonant condition of Eq. (28), and by using a large order resonance, i.e., a large integer p, one can stretch the field to times over which the control of the field parameters is more feasible. As the field strength decreases the low-l manifold becomes uncoupled from the high-l states, because of the quantum defect. Again, that is not a problem, because we turn off the driving dc field only when the electron begins to be confined in the desired high-l manifold. Finally, in our prescription we do not require a specific dependence on time of the field strength and rotation frequency, and we have given explicit

expressions only as an example. On the contrary, the functional form of the parameters of the field can be chosen in the experimentally most convenient way.

Our second scheme is based on a simple dc pulse, orthogonal to the original Stark field. The time at which the orthogonal field is applied is set according to the dynamics of the expectation value of the angular momentum for a Stark wave packet. In this respect our method closely resembles the one proposed by Ivanov and Stolow,[23] and the particulars of the excitation of the Stark manifold may be important. The crucial difference is that we use a crossed electric dc pulse instead of a magnetic field. Our final states are Stark eigenstates, and the electron can be effectively locked in the high-l manifold by enforcing cylindrical symmetry with an applied dc field. We have discussed in detail the difference between our scheme and the one proposed by Baranov *et al.*[37] in the preceding sections. Here it suffices to say that we are able to give explicit conditions [see Eqs. (34)] for the area of the crossed dc pulse that best enhances the angular momentum of the electron. The simplicity of the fields configuration and time dependence makes the crossed field scheme more convenient when very short pulses are necessary, that is, when relatively low-n Rydberg manifold are involved.

Finally, in the crossed pulse scheme, we must rely on the dynamics of the expectation value of the angular momentum, rather than of the whole state. It is not possible to estimate accurately the fraction of ZEKE electrons that remain trapped in the low-l states. Therefore, the rotating field method, which is based on the exact dynamics of the individual Stark states, should always be preferred whenever it is possible to obtain good control of the parameters of the field.

ACKNOWLEDGMENTS

We thank T. Uzer for suggesting the problem to us. We also thank him, J. Bromage, and especially W. A. Chupka for useful comments. This work was supported in part by NSF Grant No. PHY94-15583 and by the U.S. Army Research Office.

[1] K. Müller-Dethlefs, M. Sander, and E. W. Schlag, Z. Naturforsch. Teil A **39**, 1089 (1984).
[2] K. Müller-Dethlefs and E. W. Schlag, Annu. Rev. Phys. Chem. **42**, 109 (1991).
[3] E. W. Schlag, W. B. Peatman, and K. Müller-Dethlefs, J. Electron Spectrosc. Relat. Phenom. **66**, 139 (1993).
[4] D. M. Villeneuve, I. Fischer, A. Zavriyev, and A. Stolow, J. Chem. Phys. **107**, 5310 (1997).
[5] H. A. Bethe and E. E. Salpeter, *Quantum Mechanics of One- and Two-Electron Atoms* (Plenum, New York, 1977).
[6] T. F. Gallagher, *Rydberg Atoms* (Cambridge University Press, Cambridge, 1994).
[7] G. Reiser, W. Habenicht, K. Müller-Dethlefs, and E. W. Schlag, Chem. Phys. Lett. **152**, 119 (1988).
[8] K. Müller-Dethlefs, J. Chem. Phys. **95**, 4821 (1991).
[9] M. J. J. Vrakking and T. Y. Lee, Phys. Rev. A **51**, R894 (1995).
[10] M. J. J. Vrakking and T. Y. Lee, J. Chem. Phys. **102**, 8818 (1995).
[11] P. Bellomo, D. Farrelly, and T. Uzer, J. Phys. Chem. **101**, 8902 (1997).
[12] E. Rabani, R. D. Levine, A. Mühlpfordt, and U. Even, J. Chem. Phys. **102**, 1619 (1995).
[13] W. A. Chupka, J. Chem. Phys. **98**, 4520 (1993).
[14] W. A. Chupka, J. Chem. Phys. **99**, 5800 (1993).
[15] F. Merkt and R. N. Zare, J. Chem. Phys. **101**, 3495 (1994).
[16] H. Palm and F. Merkt, Chem. Phys. Lett. **270**, 1 (1997).
[17] P. Bellomo, D. Farrelly, and T. Uzer, J. Chem. Phys. **107**, 2499 (1997).
[18] P. Bellomo, D. Farrelly, and T. Uzer, J. Chem. Phys. **108**, 5295 (1998).
[19] D. L. Dorofeev and B. A. Zon, J. Chem. Phys. **106**, 9609 (1997).
[20] F. Merkt and H. Schmutz, J. Phys. Chem. **108**, 10 033 (1998).
[21] E. Lee, D. Farrelly, and T. Uzer, Chem. Phys. Lett. **231**, 241 (1994).
[22] A. Mühlpfordt, U. Even, E. Rabani, and R. D. Levine, Phys. Rev. A **51**, 3922 (1995).
[23] M. Y. Ivanov and A. Stolow, Chem. Phys. Lett. **265**, 231 (1997).
[24] R. R. Jones, P. Fu, and T. F. Gallagher, J. Chem. Phys. **106**, 3578 (1997).
[25] P. Bellomo, D. Farrelly, and T. Uzer, J. Chem. Phys. **108**, 402 (1998).
[26] P. Bellomo and C. R. Stroud, Jr., Phys. Rev. A **59**, 2139 (1999).
[27] Y. N. Demkov, B. S. Monozon, and V. N. Ostrovsky, Sov. Phys. JETP **30**, 775 (1970).
[28] Y. N. Demkov, V. N. Ostrovsky, and E. A. Solov'ev, Sov. Phys. JETP **39**, 57 (1974).
[29] W. Pauli, Z. Phys. **36**, 336 (1926).
[30] M. J. Englefield, *Group Theory and the Coulomb Problem* (Wiley, New York, 1972).
[31] M. R. W. Bellermann, P. M. Koch, and D. Richards, Phys. Rev. Lett. **78**, 3840 (1997).
[32] R. N. Zare, *Angular Momentum* (Wiley, New York, 1988).
[33] J. J. Sakurai, *Modern Quantum Mechanics* (Addison–Wesley, New York, 1985).
[34] D. Park, Z. Phys. **159**, 155 (1960).
[35] M. Born, *Mechanics of the Atom* (Bell, London, 1960).
[36] H. Goldstein, *Classical Mechanics*, 2nd ed. (Addison–Wesley, Reading, 1980).
[37] L. Y. Baranov, A. Held, H. L. Selzle, and E. W. Schlag, Chem. Phys. Lett. **291**, 311 (1988).
[38] A. Held, L. Y. Baranov, H. L. Selzle, and E. W. Schlag, Chem. Phys. Lett. **291**, 318 (1988).
[39] J. A. West, Ph.D. thesis, The Institute of Optics, University of Rochester, Rochester, New York, 1997.
[40] W. A. Chupka (private communication).